Electronic Supplementary Information (ESI)

High Performance Gas Adsorption and Natural Gas Purification in Two Microporous Metal-Organic Frameworks with Ternary Building Units

Dongmei Wang, Tingting Zhao, Yu Cao, Shuo Yao, Guanghua Li, Qisheng Huo, and Yunling Liu*

State Key Laboratory of Inorganic Synthesis and Preparative Chemistry, College of Chemistry, Jilin University, Changchun 130012, P. R. China

Materials and Methods

All the reagents were obtained from commercial sources and used without further purification. Powder X-ray diffraction (PXRD) data were collected on a Rigaku D/max-2550 diffractometer with CuKα radiation (λ = 1.5418 Å). The elemental analyses were performed on a Perkin-Elmer 2400 element analyzer. The infrared (IR) spectra were recorded within the 4000-400 cm^{-1} region on a Nicolet Impact 410 FTIR spectrometer with KBr pellets. Thermogravimetric (TG) analyses were performed on TGA Q500 V20.10 Build 36 thermogravimetric analyzer in the temperature range 35-800 °C under air flow with the heating rate of 10 $^{o}C\ min^{-1}$. Gas sorption isotherm measurements were carried out on a Micromeritics ASAP 2420 and Micromeritics ASAP 2020 instrument.

Synthesis of Compound JLU-Liu5

A mixture of $In(NO_3)_3 \cdot 4H_2O$ (15 mg, 0.05 mmol), H_5L (4.5 mg, 0.01 mmol), NMF (2 mL), and HBF_4 (0.2 mL) were added to a vial, and the solution was heated to 85℃ for 3d. Colorless crystals were collected and air-dried (70% yield based on

$In(NO_3)_3·4H_2O$). The agreement between the experimental and simulated PXRD patterns indicated the phase-purity of the as-synthesized product (see Figure S7a). ICP and elemental analysis calcd (%) for **JLU-Liu5**, $[CH_3NH_3][In_3L_2(H_2O)_{2.5}]·8NMF$: C, 42.39; H, 3.89; N, 7.06; In, 19.30; Found: C, 41.72; H, 3.96; N, 7.58; In, 19.71.

Synthesis of Compound JLU-Liu6

A mixture of $Zn(NO_3)_2·6H_2O$ (12 mg, 0.04 mmol), H_5L (4 mg, 0.01 mmol), DMF (1 mL), and HCOOH (0.05 mL) were added to a vial, and the solution was heated to 85℃for 3d. Colorless crystals were collected and air-dried (67% yield based on $Zn(NO_3)_2·6H_2O$). The agreement between the experimental and simulated PXRD patterns indicated the phase-purity of the as-synthesized product (see Figure S7b). ICP and elemental analysis calcd (%) for **JLU-Liu6**, $[(CH_3)_2NH_2][Zn_5L_2(OH)(H_2O)(DMF)_2]$: C, 44.88; H, 2.99; N, 2.90; Zn, 22.63; Found: C, 43.81; H, 3.05; N, 3.08; Zn, 22.86.

Single Crystal X-ray Structure Determination

Data were collected on a Bruker Apex II CCD diffractometer at 293(2) K for **JLU-Liu5**, with graphite-monochromated MoKα radiation (λ = 0.71073 Å). Data was performed on a Rigaku RAXIS-RAPID IP diffractometer by using graphite-monochromated Mo-Kα radiation (λ = 0.71073 Å) for **JLU-Liu6**. The structure was solved by direct methods and refined by full-matrix least-squares methods with SHELXTL.[1] All non-hydrogen atoms were easily found from the difference Fourier map. All non-hydrogen atoms were refined anisotropically. PLATON/SQUEEZE[2] was employed to calculate the diffraction contribution of the solvent molecules and, thereby, to produce a set of solvent-free diffraction intensities; structures were then refined again using the generated data. Since the highly disordered cations and guest molecules were trapped in the channels of **JLU-Liu5** and **JLU-Liu6** and could not be modeled properly, there are "Alert level A" about "Check Reported Molecular Weight" and "VERY LARGE Solvent Accessible VOID(S) in Structure" in the

"checkCIF/PLATON report" files for **JLU-Liu5** and **JLU-Liu6**. The final formulas of **JLU-Liu5** and **JLU-Liu6** were derived from crystallographic data combined with elemental and thermogravimetric analysis data. The CCDC-1000072-1000073 contain the supplementary crystallographic data for this paper. These data can be obtained free of charge from the Cambridge Crystallographic Data Centre via www.ccdc.cam.ac.uk/data_request/cif. Basic information pertaining to crystal parameters and structure refinement is summarized in Table S1, and selected bond lengths [Å] and angles [º] are listed in Table S6 and Table S7.

Table S1 Crystal data and structure refinement for the two compounds.

Name	**JLU-Liu5**	**JLU-Liu6**
pirical formula	$C_{63}H_{69}In_3N_9O_{30.50}$	$C_{54}H_{43}N_3O_{24}Zn_5$
Formula weight	1784.73	1444.76
Temperature (K)	296(2)	293(2)
Wave length (Å)	0.71073	0.71073
Crystal system	Orthorhombic	Monoclinic
Space group	Fdd2	c2/c
a (Å)	33.493(5)	29.372(6)
b (Å)	53.707(8)	15.784(3)
c (Å)	22.036(3)	19.140(4)
α (deg)	90	90
β (deg)	90	107.16(3)
γ (deg)	90	90
Volume ($Å^3$)	39639(10)	8478(3)
Z, D_{calc} (Mg/m^3)	16, 1.196	4, 1.132
Absorption coefficient (mm^{-1})	0.760	1.452
F (000)	14416	2920
Crystal size (mm^3)	0.38 x 0.26 x 0.24	0.27 x 0.26 x 0.24
θ range (deg)	1.17 to 25.00	3.07 to 27.46
index range (deg)	-32<=h<=39,-63<=k<=63, -26<=l<=19	-38<=h<=37,-20<=k<=20, -24<=l<=24
Reflections collected / unique	42211 / 14946 [R(int) = 0.0660]	40113 / 9621 [R(int) = 0.0574]
Data / restraints / parameters	14946 / 37 / 645	9621 / 18 / 424
Goodness-of-fit on F^2	1.089	1.089
R_1, wR_2 ($I>2\sigma(I)$)	0.0603, 0.1676	0.0715, 0.2301
R_1, wR_2 (all data)	0.0737, 0.1742	0.0952, 0.2436
Largest diff. peak and hole (e $Å^{-3}$)	0.940, -0.834	2.865, -1.184

$R_1=\sum||F_o|-|F_c||/\sum|F_o|$. $wR_2=[\sum[\ w\ (F_o^2-F_c^2)^2]\ /\ \sum[\ w\ (F_o^2)^2]]^{1/2}$

Fig. S1 Three types of 5-connected ligands with different dihedral angles in **JLU-Liu5** (a, b) and **JLU-Liu6** (c).

Fig. S2 The structure of **JLU-Liu5**: a) 3D framework with different direction metal-organic square (MOS) linked by ligands; b) 1D chain with distorted MOS; c) 1D tube along [011] direction.

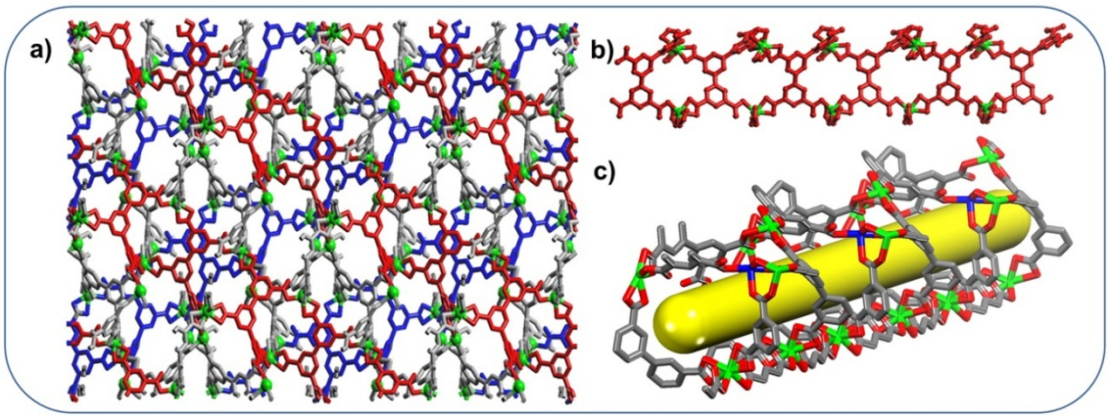

Fig. S3 The structure of **JLU-Liu6**: (a) 2D chain along [101] direction; (b) Stick and ball model of the 3D framework along the [110] direction.

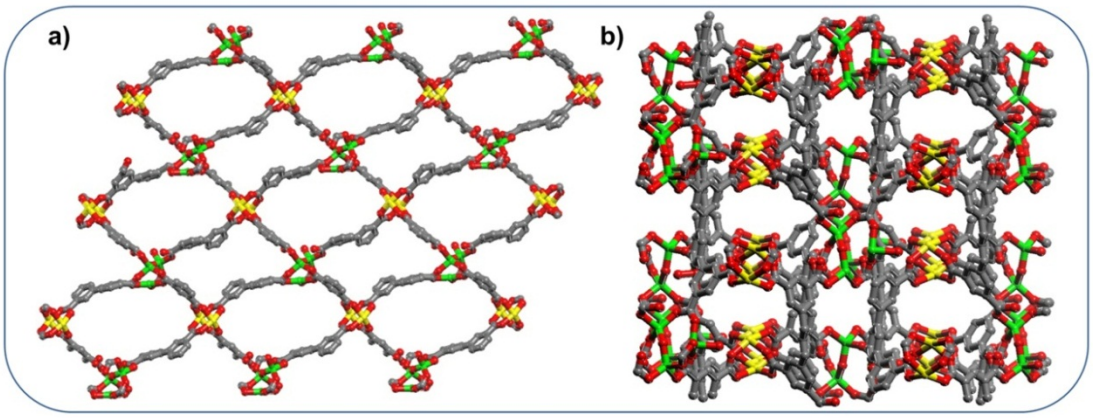

Topology Analysis

The two compounds are assembled by one kind of organic SBU and two kinds of inorganic SBUs, when considering the H_5L ligand as 5-c nodes, **JLU-Liu5** and **JLU-Liu6** can be regarded as novel (4,5)-c and (4,5,6)-c nets, respectively (Fig. S4a, S5a). However, preferable description could be obtained as below: the organic H_5L linker can be considered as three 3-c nodes centered between three phenyl rings, leading to the different new (3,4)-c and (3,4,6)-c nets for the compounds **JLU-Liu5** and **JLU-Liu6**, respectively (Fig. S4b, S5b). The topological information for two compounds is summarized in Table S2.

Fig. S4 Illustration of topology of **JLU-Liu5**: simplification of the inorganic $In(CO_2)_4$ (4-connected node, green) and $In_2(H_2O)(CO_2)_4$ clusters (4-connected node, blue), and the organic H_5L linker (5-connected nodes, purple), leading to the new (4,5)-c net a). When the organic H_5L linker was regarded as three 3-connected nodes (purple), lead to the new (3,4)-c net b). Hydrogen atoms are omitted for clarity.

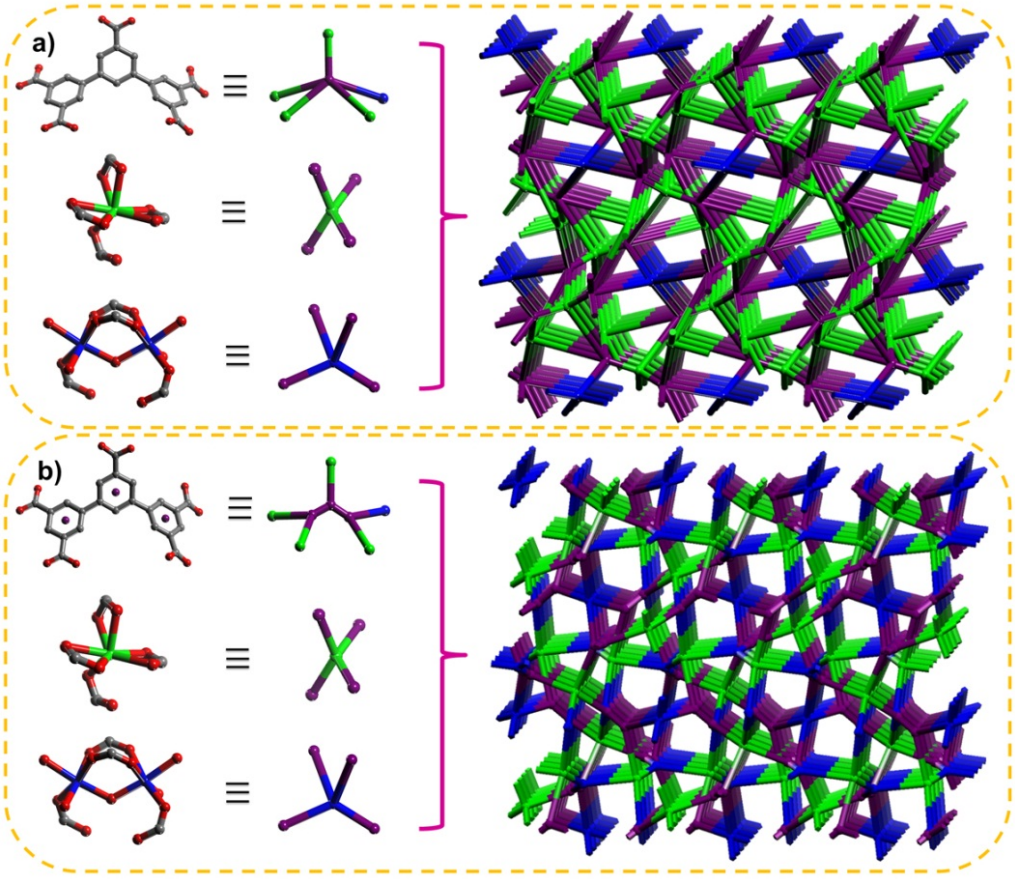

Fig. S5 Illustration of topology of **JLU-Liu6**: simplification of the inorganic $Zn_2(CO_2)_4$ paddlewheels (4-connected node, yellow) and $Zn_3(CO_2)_6$ clusters (6-connected node, green), and the organic H_5L linker (5-connected nodes, purple), leading to the new (4,5,6)-c net a). When the organic H_5L linker regarded as three 3-connected nodes (purple), leading to the new (3,4,6)-c net b). Hydrogen atoms are omitted for clarity.

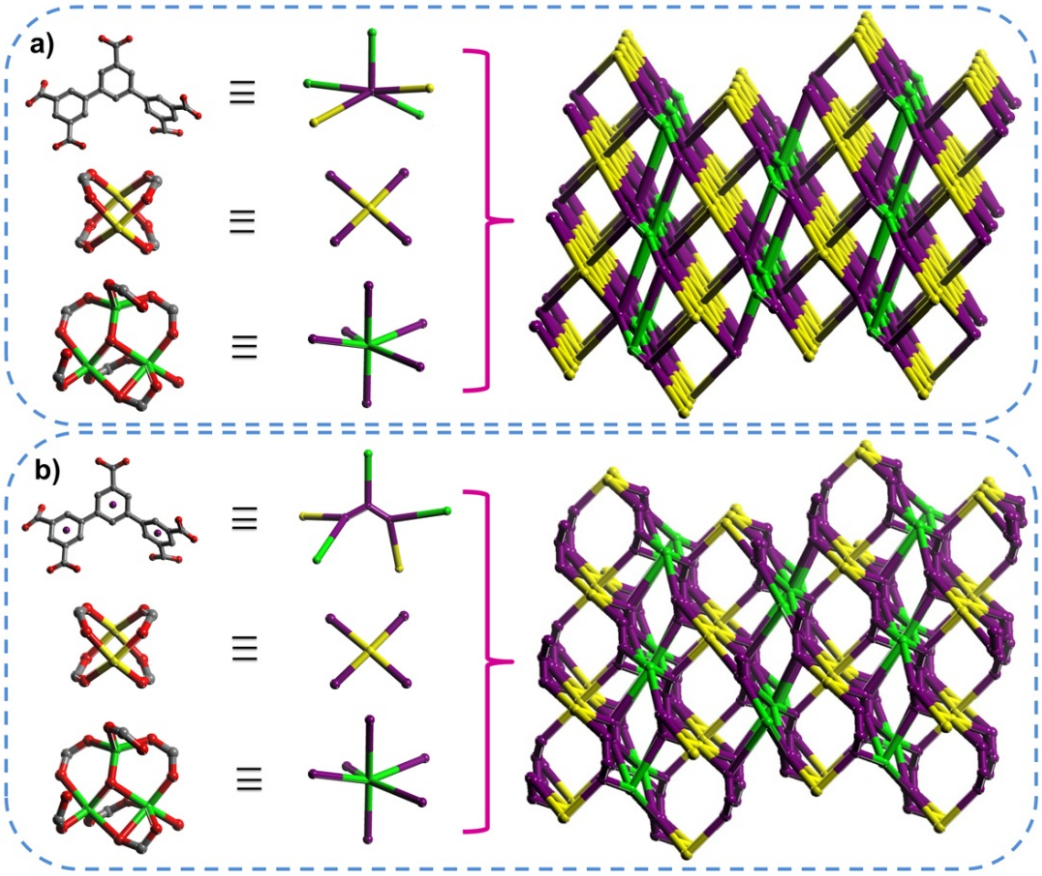

Table S2 The topological information for **JLU-Liu5a** (4,5)-c net and **JLU-Liu5b** (3,4)-c net, and **JLU-Liu6a** (4,5,6)-c net and **JLU-Liu6b** (3,4,6)-c net calculated by *Topos 4.0* and *Systre*.

Compound **JLU-Liu5a**

Vertex figure	**Square pyramid + Tetrahedron**										
Vertex	**CS1**	**CS2**	**CS3**	**CS4**	**CS5**	**CS6**	**CS7**	**CS8**	**CS9**	**CS10**	**Cum10**
V_1(square pyramid)	5	13	33	47	96	117	202	218	350	350	1432
V_2(square pyramid)	5	11	31	47	91	109	196	212	342	345	1389
V_3(tetrahedron)	4	16	26	56	78	150	168	278	282	282	1502
V_4(tetrahedron)	4	14	25	55	72	134	154	260	273	273	1423
V_5(tetrahedron)	4	14	26	61	76	137	160	271	278	278	1461
Vertex	**Extended point symbols**										
V_1(square pyramid)	[4(2).4(2).6.6.6.6(2).6(2).6(2).6(2).6(3)]										
V_2(square pyramid)	[4(2).6.6.6.6.6(2).6(2).6(2).6(3).6(3)]										
V_3(tetrahedron)	[6(2).6(2).6(2).6(2).6(4).6(4)]										
V_4(tetrahedron)	[4.6.4.6(3).4.6(3)]										
V_5(tetrahedron)	[4.6.4.6(2).4.6(4)]										

Compound **JLU-Liu5b**

Vertex figure	**Triangle + Tetrahedron**										
Vertex	**CS1**	**CS2**	**CS3**	**CS4**	**CS5**	**CS6**	**CS7**	**CS8**	**CS9**	**CS10**	**Cum10**
V_1(Triangle)	3	7	18	29	53	74	109	136	193	227	849
V_2(Triangle)	3	8	17	33	52	74	110	142	189	233	861
V_3(Triangle)	3	8	17	32	55	80	106	150	184	246	881
V_4(Triangle)	3	8	17	32	52	82	110	155	181	245	885
V_5(Triangle)	3	8	17	32	51	82	106	149	177	247	872
V_6(tetrahedron)	4	8	20	36	56	76	116	144	204	232	896
V_7(tetrahedron)	4	8	18	36	53	79	114	145	194	241	892
V_8(Triangle)	3	7	18	30	53	74	104	146	180	230	845
V_9(tetrahedron)	4	8	20	32	57	84	117	144	202	235	903
Vertex	**Extended point symbols**										
V_1(Triangle)	[7.7.7]										
V_2(Triangle)	[7.7.9(3)]										
V_3(Triangle)	[7.7(2).8(2)]										
V_4(Triangle)	[7.7.7(2)]										
V_5(Triangle)	[7.7.7]										
V_6(tetrahedron)	[7.7.8.8.8(2).9(2)]										
V_7(tetrahedron)	[7.7.7.7.9.8]										

V_8(Triangle)	[7.7(2).8]
V_9(tetrahedron)	[7.7.7.7.7.8]

Compound **JLU-Liu6a**

Vertex figure	**Square + Square pyramid + Octahedron**										
Vertex	**CS1**	**CS2**	**CS3**	**CS4**	**CS5**	**CS6**	**CS7**	**CS8**	**CS9**	**CS10**	**Cum10**
V_1(square)	5	16	35	63	97	140	189	248	312	387	1492
V_2(square pyramid)	4	14	36	60	94	136	190	244	308	382	1468
V_3(octahedron)	6	16	34	62	100	140	188	246	316	386	1494
Vertex	**Extended point symbols**										
V_1(square)	[4.4.4.4.4.6(2).6(2).6(4).6(5).6]										
V_2(square pyramid)	[4.4.6(2).8(20).6(3).6(3)]										
V_3(octahedron)	[4.4.4.4.4.4.4.6(4).6(4).6(4).6(4).6.6.6(2)]										

Compound **JLU-Liu6b**

Vertex figure	**Triangle + Square +Octahedron**										
Vertex	**CS1**	**CS2**	**CS3**	**CS4**	**CS5**	**CS6**	**CS7**	**CS8**	**CS9**	**CS10**	**Cum10**
V_1(octahedron)	6	12	24	44	82	108	138	188	266	286	1154
V_2(Triangle)	3	10	22	42	67	103	138	190	232	303	1110
V_3(Triangle)	3	10	22	44	69	101	142	190	233	299	1113
V_4(Triangle)	3	9	24	38	69	104	142	176	238	303	1106
V_5(Square)	4	8	28	46	66	98	160	184	234	294	1122
Vertex	**Extended point symbols**										
V_1(octahedron)	[6.6.6.6.7.7.7.7.7.7.7(2).8.8.8.9(2)]										
V_2(Triangle)	[6.7.7(2)]										
V_3(Triangle)	[6.7.7(2)]										
V_4(Triangle)	[6.6.7]										
V_5(Square)	[7(3).7(3).8(2).8(2).9(2).9(2)]										

Fig. S6 Infrared spectra for the two compounds **JLU-Liu5** and **JLU-Liu6** (KBr, cm^{-1}).

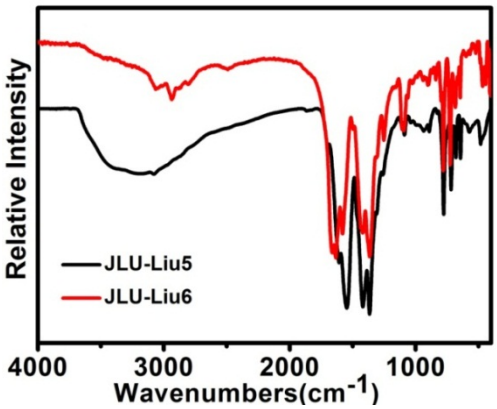

Fig. S7 Experimental and calculated powder X-ray diffraction (PXRD) patterns for

the two compounds **JLU-Liu5** (a) and **JLU-Liu6 (**b), indicating the phase purity of the as-synthesized, solvent exchanged and activated samples.

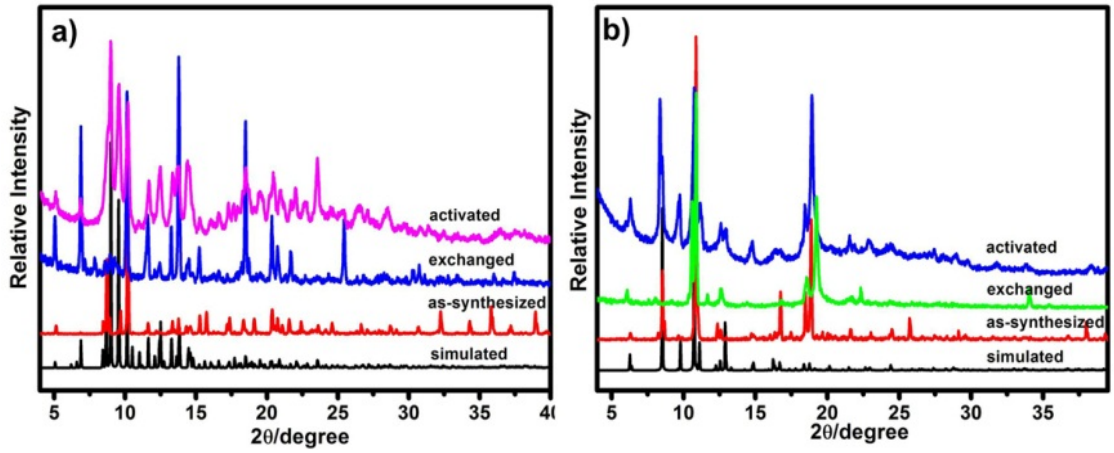

Fig. S8 Thermogravimetric analysis curves for the as-synthesized and exchanged compounds (a) **JLU-Liu5** exchanged with CH_3COCH_3 and (b) **JLU-Liu6** exchanged with CH_2Cl_2.

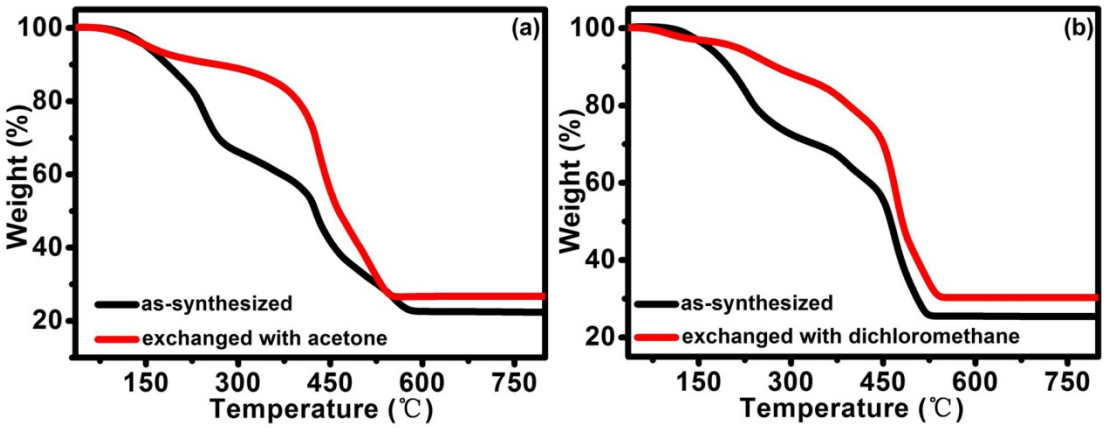

Thermogravimetric Analysis

Thermogravimetric analysis (TGA) for the compound **JLU-Liu5** shows a weight loss of 29.8 % between 35 and 260 ^oC, which corresponding to the loss of $CH_3NH_3^+$ and coordinated two and half H_2O molecules and eight NMF molecules (calcd: 30.8 %). The further weight loss of 50.9% occurs between 260 and 600^oC should be attributed to the release of organic H_5L ligands (calcd 49.9%). The profiles for acetone exchanged materials indicated that the guest NMF and coordinated water molecules captured in the pore were mostly removed, and the framework of **JLU-Liu5** was stable to 350^oC. PXRD studies indicated that the final product, upon

calcinations above 600°C, is a main phase of In_2O_3 (JCPDS: 71-2194).

Thermogravimetric analysis (TGA) for the compound **JLU-Liu6** shows a weight loss of 16.2 % between 35 and 220°C, which corresponding to the loss of $(CH_3)_2NH_2^+$ and coordinated H_2O molecule and two DMF molecules (calcd: 15.4 %). The further weight loss of 62% between 220 and 520°C, and should be attributed to OH^- and the release of organic H_5L ligands (calcd 62.8%). The profiles for dichloromethane exchanged materials indicated that the coordinated water and DMF molecules were mostly removed, and the framework of **JLU-Liu6** was stable to 350°C. PXRD studies indicated that the final product, upon calcinations above 600°C, is a dense phase of ZnO (JCPDS: 36-1451).

Gas sorption measurements.

In the two compounds, the different degree of distortion of the unsymmetrical pentacarboxylate ligand results in the formation of the multiple-pore system with pore sizes ranging from 5.9 to 13.5 Å, such materials with multiple pores are often applied to the field of gas adsorption and separation. In addition, the two compounds are anionic framework, and the counter-cations, $CH_3NH_3^+$, $(CH_3)_2NH_2^+$ which came from the decomposition of the solvent NMF molecules and DMF molecules, occupied in the pores for charge balance of the framework of **JLU-Liu5** and **JLU-Liu6**, respectively. The counter-cations and open metal sites (OMSs) generated by thermal activation obviously influence gas adsorption and separation. The accessible pore volumes of the structures were estimated to be 66.7% for **JLU-Liu5** and 56.4% for **JLU-Liu6** of the total volume without the guest molecules and counter-cations in the pores, according to calculations using PLATON.

Before the gas sorption isotherm measurements, the as-synthesized **JLU-Liu5** and **JLU-Liu6** samples were solvent-exchanged with acetone and dichloromethane for 2 days, respectively. The solvent exchanged sample was then dried at 80°C under vacuum overnight lead to the formation of activated sample. The activated samples still maintain high crystallinity, as evidenced by the PXRD patterns (Fig. S7). About 100 mg of the desolvated samples were used for the entire adsorption/desorption

measurements.

Table S3 Gas adsorption data of compounds **JLU-Liu5** and **JLU-Liu6**.

		H_2[b]		CO_2[b]		CH_4[b]		C_2H_6[b]		C_3H_8[b]	
MOFs	SA_{BET}[a]	77K	87K	273K	298K	273K	298K	273K	298K	273K	298K
JLU-Liu5	707	163	127	102	52	28	16	90	71	78	70
JLU-Liu6	544	150	124	70	43	24	13	62	49	62	57

[a] Surface area ($m^2\ g^{-1}$) was calculated from N_2 isotherm. [b] Gas uptake in $cm^3\ g^{-1}$.

Fig. S9 (a) Nitrogen sorption isotherms on **JLU-Liu5** (red) and **JLU-Liu6** (blue) at 77 K. (b) The pore size distribution calculated using the DFT method. Adsorption: closed symbols; desorption: open symbols, respectively.

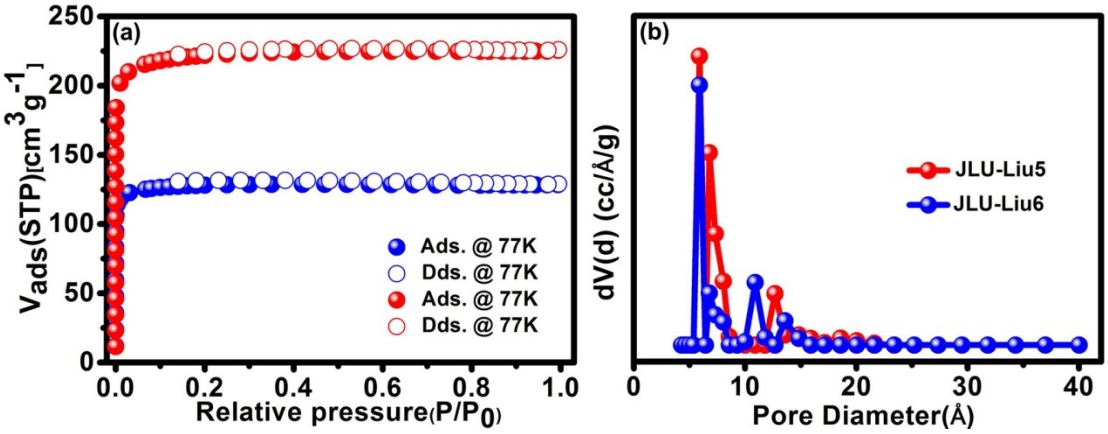

Fig. S10 Hydrogen adsorption isotherms for the two compounds **JLU-Liu5** (a) and **JLU-Liu6** (b).

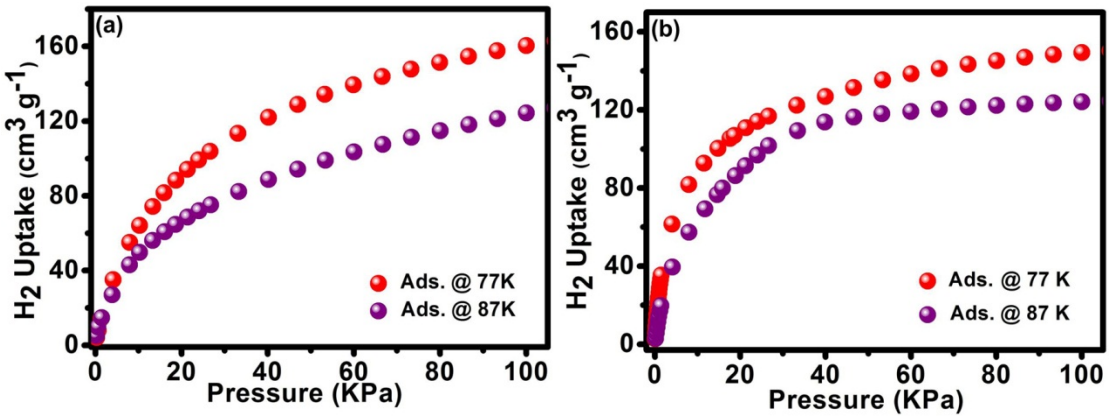

Calculations of the Isosteric Heats of Gas Adsorption (Q_{st}):

A virial-type[4] expression comprising the temperature-independent parameters a_i and b_j was employed to calculate the enthalpies of adsorption for CH_4, C_2H_6 and C_3H_8 (at 273 and 298 K) on compounds. In each case, the data were fitted using the equation:

$$ln^P = ln^N + {}^1/_T \sum_{i-0}^{m} a_i N^i + \sum_{j-0}^{n} b_j N^j$$

Here, P is the pressure expressed in Torr, N is the amount adsorbed in mmol g^{-1}, T is the temperature in K, a_i and b_j are virial coefficients, m, n represent the number of coefficients required to adequately describe the isotherms (m and n were gradually increased until the contribution of extra added a and b coefficients was deemed to be statistically insignificant towards the overall fit, and the average value of the squared deviations from the experimental values was minimized). The values of the virial coefficients a_0 through a_m were then used to calculate the isosteric heat of adsorption using the following expression.

$$Q_{st} = -R \sum_{i-0}^{m} a_i N^i$$

Q_{st} is the coverage-dependent isosteric heat of adsorption and R is the universal gas constant. The heat of gas sorption for **JLU-Liu5** and **JLU-Liu6** in this manuscript are determined by using the sorption data measured in the pressure range from 0-1 bar (273 and 298 K for gases), which is fitted by the virial-equation very well.

Fig. S11 (a) Nonlinear curves fitting of CO_2 for **JLU-Liu5** at 273 K and 298 K; (b) Isosteric heat of CO_2 for **JLU-Liu5**.

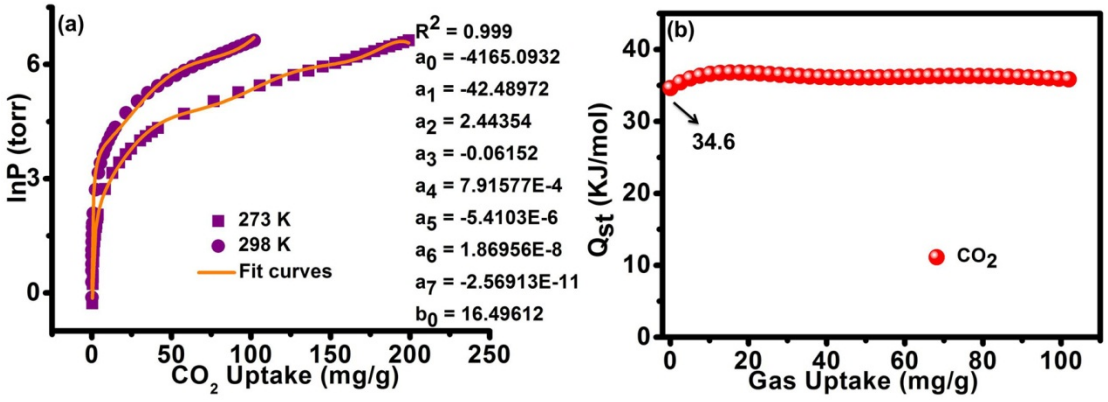

Fig. S12 (a) Nonlinear curves fitting of C_3H_8 for **JLU-Liu5** at 273 K and 298 K; (b) Isosteric heat of C_3H_8 for **JLU-Liu5**.

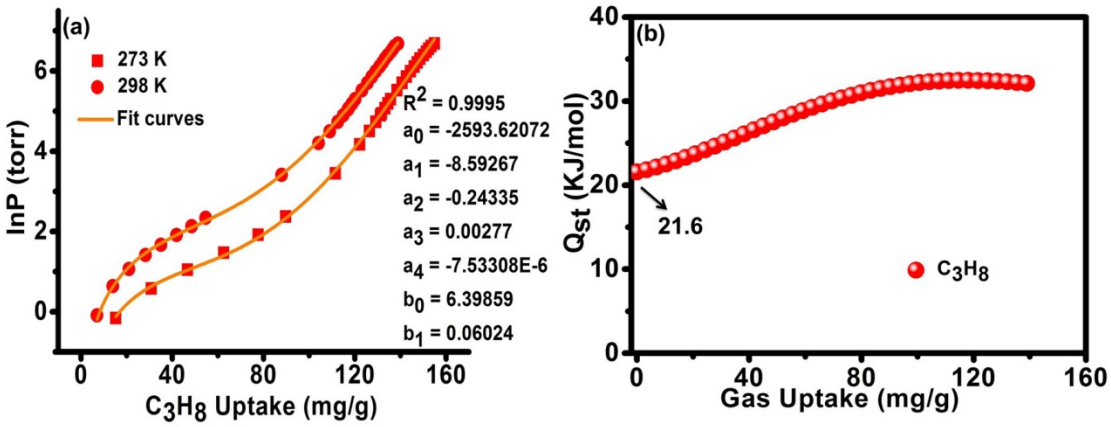

Fig. S13 (a) Nonlinear curves fitting of C_2H_6 for **JLU-Liu5** at 273 K and 298 K; (b) Isosteric heat of C_2H_6 for **JLU-Liu5**.

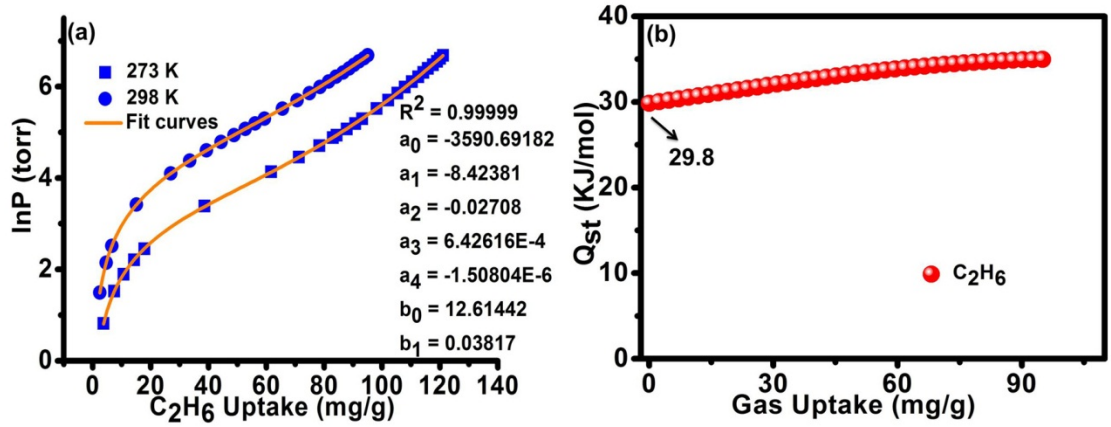

Fig. S14 (a) Nonlinear curves fitting of CH_4 for **JLU-Liu5** at 273 K and 298 K; (b) Isosteric heat of CH_4 for **JLU-Liu5**.

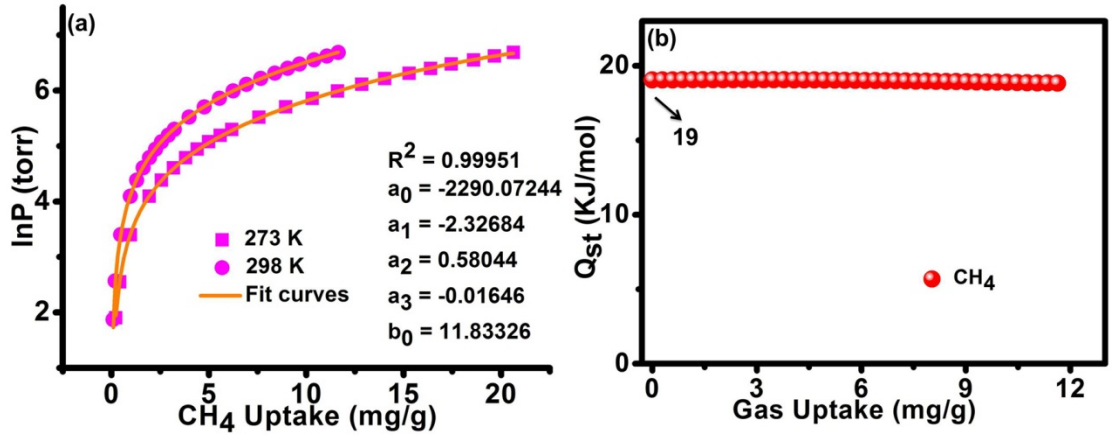

Fig. S15 (a) Nonlinear curves fitting of CO_2 for **JLU-Liu6** at 273 K and 298 K; (b) Isosteric heat of CO_2 for **JLU-Liu6**.

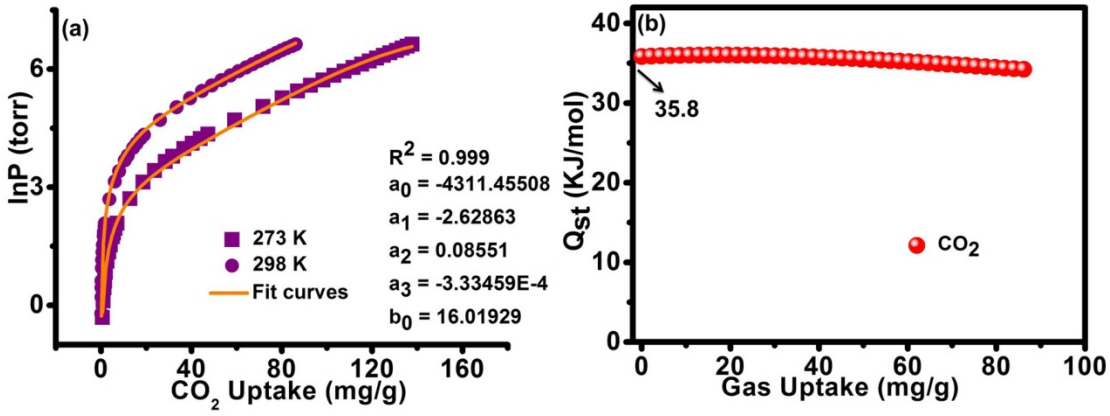

Fig. S16 (a) Nonlinear curves fitting of C_3H_8 for **JLU-Liu6** at 273 K and 298 K; (b) Isosteric heat of C_3H_8 for **JLU-Liu6**.

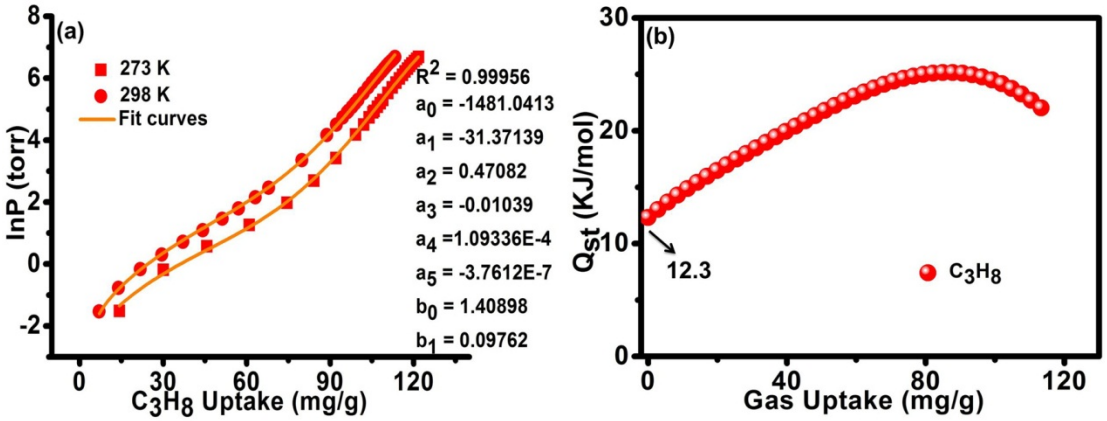

Fig. S17 (a) Nonlinear curves fitting of C_2H_6 for **JLU-Liu6** at 273 K and 298 K; (b) Isosteric heat of C_2H_6 for **JLU-Liu6**.

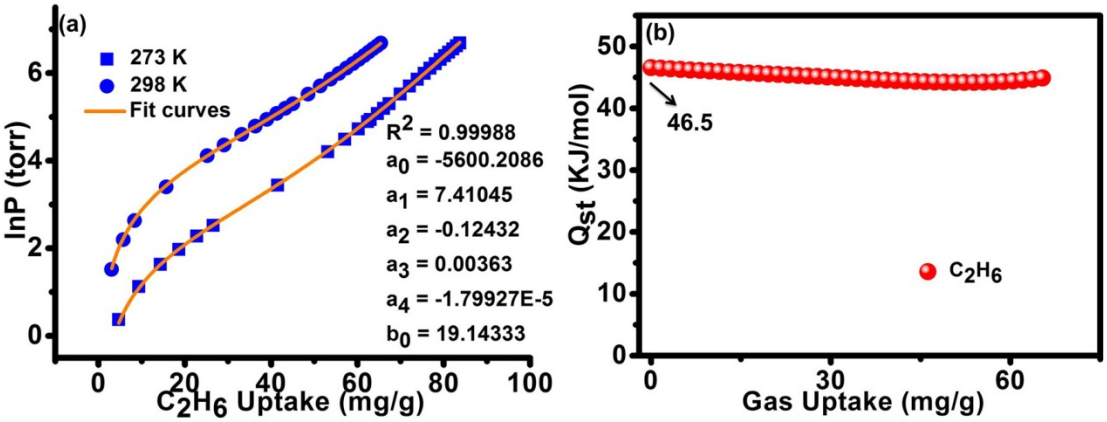

Fig. S18 (a) Nonlinear curves fitting of CH_4 for **JLU-Liu6** at 273 K and 298 K; (b)

Isosteric heat of CH_4 for **JLU-Liu6**.

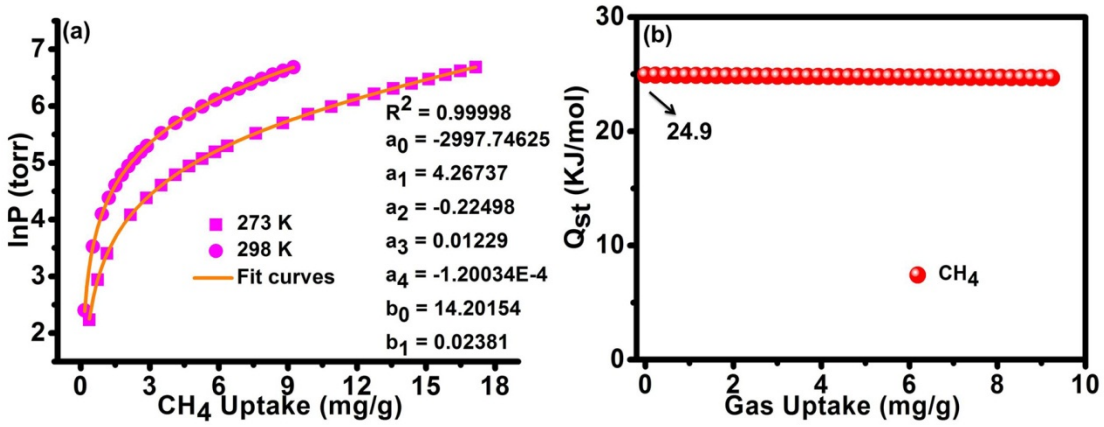

Prediction of adsorption of binary mixture by IAST theory

The excess adsorption data for pure gases measured at 298 *K*, were first converted to absolute loadings, along with *Peng-Robinson* equation. In order to perform the IAST calculations, the single-component isotherm was fitted by the dual-site Langmuir-Freundlich (DSLF) adsorption model[5] to correlate the pure-component equilibrium data and further predict the adsorption of mixtures. The DSLF model is described as:

$$N^0\ (f) = \frac{N_1 k_1 f}{1 + k_1 f} + \frac{N_2 k_2 f}{1 + k_2 f}$$

Where *f* is the fugacity of bulk gas at equilibrium with adsorbed phase, N_i is the model parameter of the maximum adsorption amount at the site *i* (*i*=1 or 2), and k_i is the affinity constant.

Based on the above model parameters of pure gas adsorption, we used the IAST model,[6] which was proposed by *Myer* and *Prausnitz* in 1965 to predict the multi-component adsorption. Analogous to *Raoult's* law for vapor-liquid equilibrium, the IAST assumes that the adsorbed solutions are ideal and all activity coefficients in the adsorbed phase are unity. Thus, the adsorption equilibrium between adsorbed and gas phases will lead to the following equation

$$Py_i\varphi_i = x_i f_i^0(\pi)$$

Where f_i^0 is the fugacity of the equilibrium gas phase corresponding to the spreading

pressure π for the adsorption of pure gas i, φ_i is the gas fugacity coefficient of component i calculated by *PR* equation of state, and x_i and y_i are the molar fraction of component i at the adsorbed and bulk phases, respectively. The binary gas mixing process is carried out at constant spreading pressure π and indicated by

$$\int_0^{f_1^0} N_1^0(f_1)dlnf_1 = \int_0^{f_2^0} N_2^0(f_2)dlnf_2$$

Where the single-component adsorption amount and selectivity are further obtained from the above equation by numerical integration and root exploration.

To investigate the separation of binary mixtures, the adsorption selectivity is defined by

$$S_{ij} = \frac{x_i / x_j}{y_i / y_j}$$

Where the selectivity refers to the first component over the second one, and the x_i, x_j and y_i, y_j denote the molar fractions of species i, j in the adsorbed and bulk phases, respectively.

Fig. S19 Isotherms of each component of CO_2/CH_4 mixture in the compound **JLU-Liu5** (a) predicted by IAST for equimolar mixtures of CO_2 and CH_4 at 298 K and 1 bar; (b) IAST selectivity of CO_2 versus CH_4 at various pressures and mole fractions of CH_4 (y_{CH4}= 0.05 and 0.95) at 298K and 1 bar; **Jlu-Liu6** for (c, d).

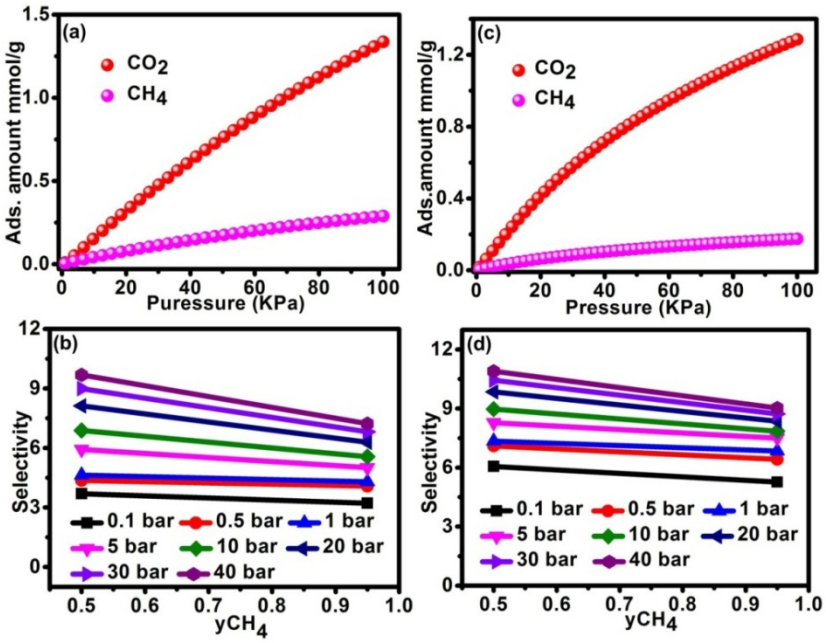

Table S4 Comparison of the two compounds with some other materials for CO_2/CH_4 adsorptive selectivity at 298 K and 1 bar.

	Compound	Selectivity	Reference
MOFs materials	MOF-177	0.9	7
	ZIF-8	1.4	7
	UMCM-1	1.8	7
	$Cu_3(BTC)_2$	2.3	7
	MIL-53(Al)	2.3	7
	MOF-5	2.3	9
	JLU-Liu5	4.6	This work
	$[Zn_2(L)]$	4.8	8
	$[Zn_2(L)(DMF)_2]$	5.7	8
	$[Zn_2(L)(py\text{-}CF_3)_2]$	6.2	8
	M'MOF-20a	6.8	9
	JLU-Liu6	7.4	This work
	PAF-1-450	7.9	10
	$Zn_5(BTA)_6(TDA)_2$ 15DMF $8H_2O$	9.2	11
	$[Cu(bpy\text{-}1)_2SiF_6]$	10.5	12
	$[Cu_2(HBTB)_2(H_2O)(EtOH)]$ H_2O EtOH	12	13

	MPM-1-TIFSIX	20.3	14
Carbon materials	a-MCMBs	3.7	15
	activated carbon	3.7	15
	C_{168}	5.4	16
	activated carbon bead	1.9	16

Fig. S20 Measured CO_2 and N_2 isotherms at 298 K along with the DSLF fits for **JLU-Liu5** (a) and **JLU-Liu6** (d); Isotherms of each component of CO_2/N_2 mixture in **JLU-Liu5** (b) and **JLU-Liu6** (e) predicted by IAST for equimolar mixtures of CO_2 and N_2 at 298 K and 1 bar; IAST predicted equimolar gas mixture adsorption selectivities at 298K and 1 bar for **JLU-Liu5** (c) and **JLU-Liu6** (f).

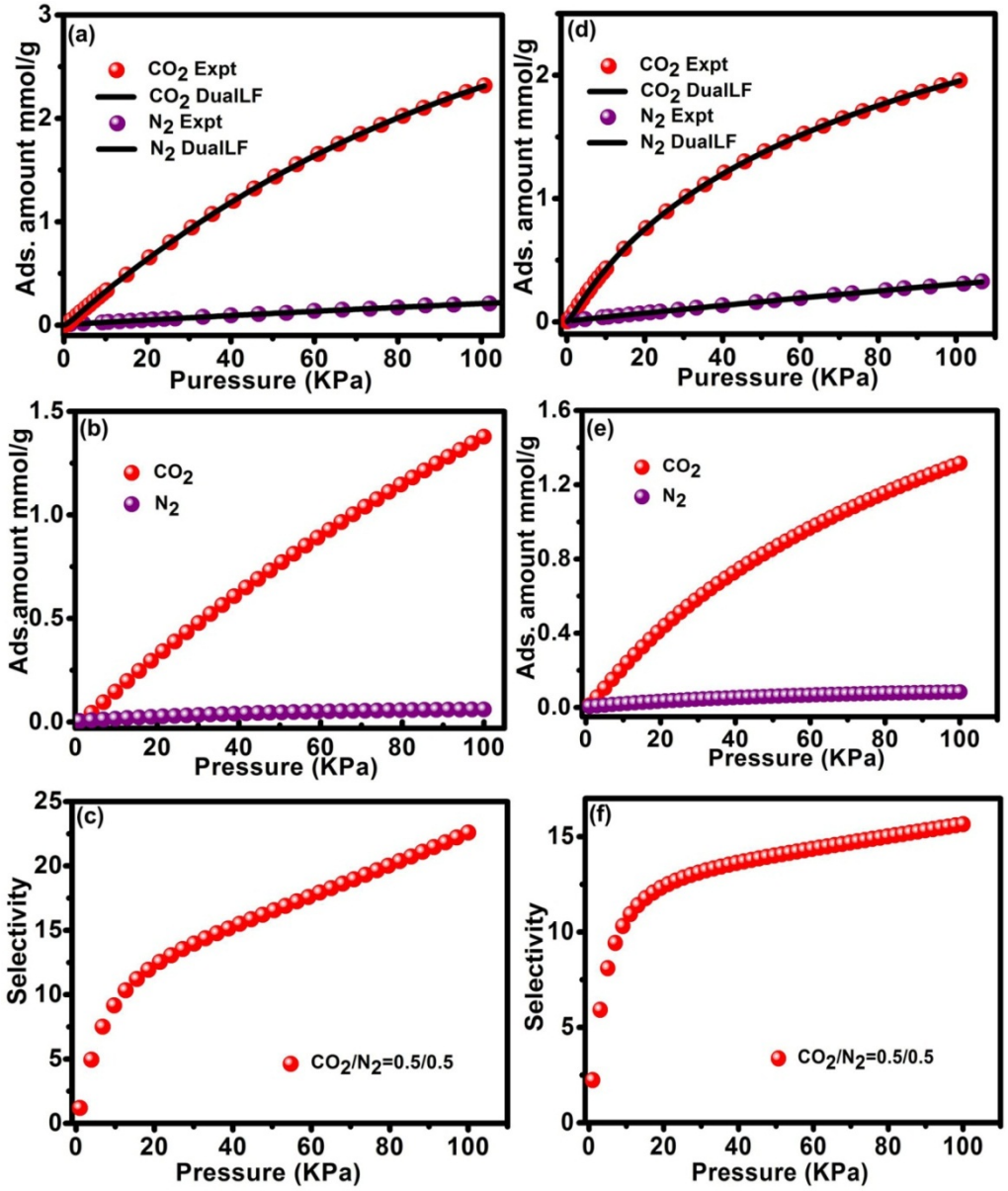

Fig. S21 Isotherms of each component of C_3H_8/CH_4 and C_2H_6/CH_4 mixture in **JLU-Liu5** (a, b) predicted by IAST for equimolar mixtures of gases at 298 K and 1 bar; **JLU-Liu6** (c, d).

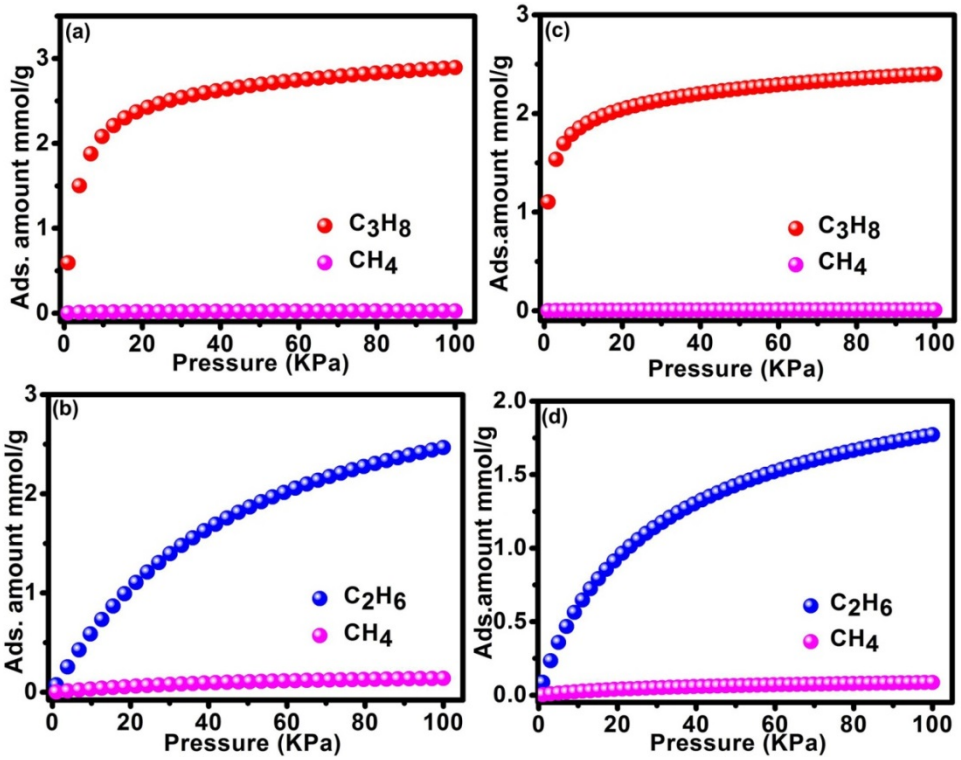

Table S5 Parameters of measured pure CO_2, CH_4, C_2H_6 and C_3H_8 isotherm at 298 K along with the DSLF fits.

adsorbent	adsorbate	N_1 [mmol g^{-1}]	k_1 [kPa^{-1}]	n_1	N_2 [mmol g^{-1}]	k_2 [kPa^{-1}]	n_2
JLU-Liu5	N_2	1.30549	0.00151	1.04061	0.00885	0.85447	0.46001
	CO_2	4.39363	0.0035	1.22409	0.12907	0.04565	1.62694
	CH_4	3.53769	0.0017	1.0752	0.00331	0.0867	4.00322
	C_2H_6	3.70116	0.01651	0.63117	2.57805	0.03074	1.18285
	C_3H_8	2.30288	0.65201	1.17237	2.83992	0.03965	0.51303
JLU-Liu6	N_2	0.80000	0.00921	0.41589	1.50000	9.7099E-4	1.16659
	CO_2	0.76959	0.03561	1.17276	2.74621	0.0047	1.12915
	CH_4	2.65699	0.00149	1.02422	0.36848	0.00936	0.9792
	C_2H_6	2.32227	0.0761	0.95659	0.38574	8.7613E-5	1.92937
	C_3H_8	1.4974	0.13433	0.54199	1.63135	2.88322	0.95232

Fig. S22 Fluorescent emission spectra of ligand H_5L (black), and **JLU-Liu5** (red),

JLU-Liu6 (green) in solid state at room temperature.

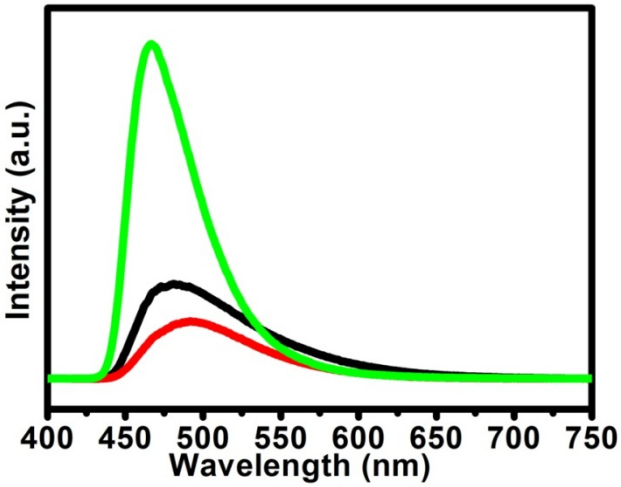

Photoluminescent Properties:

The solid-state luminescence of the two compounds **JLU-Liu5** and **JLU-Liu6**, as well as the free ligand H_5L, are investigated at room temperature. As depicted in Fig. S22, the **JLU-Liu5** and **JLU-Liu6** display fluorescent emission bands at 491 nm and 466 nm upon excitation at 396 nm and 339 nm, respectively. These bands can probably be assigned to the π-π* intraligand luminescent emission since similar emission is observed at 481 nm upon excitation at 410 nm for ligand.

Compared with the free ligand, the **JLU-Liu5** has a decreased luminescent intensity, it may results from the more coordinated water molecules which have a strong quenching effect to the luminescence. However, the luminescent intensity of **JLU-Liu6** is greatly enhanced. It probably due to the unique coordination of the ligand to the Zn^{2+} center, which increases the conformational rigidity of the ligand, thereby reduces the nonradiative decay of the intraligand (π-π*) excited state. In comparison with the emission of H_5L, slight blue-shift of 10 nm occur in the maximum emission peaks in the compound **JLU-Liu6**, and slight red-shift of 15 nm occur in the compound **JLU-Liu5**. As the ligand dominates luminescence of the compounds, the blue and red-shifted emission can be presumably associated with coordinative environment around the ligand.

Table S6. Selected bond lengths [Å] and angles [º] for compound **JLU-Liu5**.

In(1)-O(21)	2.059(5)	In(1)-O(14)#1	2.152(7)
In(1)-O(3)	2.111(6)	In(1)-O(23)	2.160(14)
In(1)-O(22)	2.139(12)	In(1)-O(13)	2.167(7)
In(2)-O(6)	2.128(7)	In(2)-O(18)#4	2.274(6)
In(2)-O(11)#2	2.179(7)	In(2)-O(1)#3	2.285(7)
In(2)-O(2)#3	2.224(6)	In(2)-O(12)#2	2.366(7)
In(2)-O(17)#4	2.259(6)	In(2)-O(5)	2.535(8)
In(3)-O(9)#5	2.130(7)	In(3)-O(15)	2.265(6)
In(3)-O(20)#6	2.195(6)	In(3)-O(7)#7	2.283(6)
In(3)-O(8)#7	2.234(6)	In(3)-O(19)#6	2.351(7)
In(3)-O(16)	2.259(6)		
O(21)-In(1)-O(3)	103.0(3)	O(22)-In(1)-O(23)	87.9(5)
O(21)-In(1)-O(22)	172.2(4)	O(14)#1-In(1)-O(23)	172.2(4)
O(3)-In(1)-O(22)	84.7(4)	O(21)-In(1)-O(13)	87.7(3)
O(21)-In(1)-O(14)#1	91.7(3)	O(3)-In(1)-O(13)	169.3(3)
O(3)-In(1)-O(14)#1	93.0(3)	O(22)-In(1)-O(13)	84.6(4)
O(22)-In(1)-O(14)#1	86.9(4)	O(14)#1-In(1)-O(13)	86.9(4)
O(21)-In(1)-O(23)	92.6(4)	O(23)-In(1)-O(13)	86.8(5)
O(3)-In(1)-O(23)	92.3(4)	O(17)#4-In(2)-O(1)#3	88.2(2)
O(6)-In(2)-O(11)#2	112.9(3)	O(18)#4-In(2)-O(1)#3	126.6(2)
O(6)-In(2)-O(2)#3	88.7(3)	O(11)#2-In(2)-O(12)#2	57.0(2)
O(11)#2-In(2)-O(2)#3	137.6(3)	O(2)#3-In(2)-O(12)#2	165.1(2)
O(6)-In(2)-O(17)#4	139.6(3)	O(17)#4-In(2)-O(12)#2	82.4(3)
O(11)#2-In(2)-O(17)#4	92.8(3)	O(18)#4-In(2)-O(12)#2	83.3(2)
O(2)#3-In(2)-O(17)#4	92.5(3)	O(1)#3-In(2)-O(12)#2	135.8(2)
O(6)-In(2)-O(18)#4	82.4(3)	O(6)-In(2)-O(5)	53.6(3)
O(11)#2-In(2)-O(18)#4	134.5(2)	O(11)#2-In(2)-O(5)	82.3(3)
O(2)#3-In(2)-O(18)#4	82.2(2)	O(2)#3-In(2)-O(5)	82.6(3)
O(17)#4-In(2)-O(18)#4	57.8(2)	O(17)#4-In(2)-O(5)	166.2(3)
O(6)-In(2)-O(1)#3	125.2(3)	O(18)#4-In(2)-O(5)	133.5(2)
O(11)#2-In(2)-O(1)#3	80.7(3)	O(1)#3-In(2)-O(5)	78.3(3)
O(2)#3-In(2)-O(1)#3	57.5(2)	O(12)#2-In(2)-O(5)	105.3(3)
O(6)-In(2)-O(12)#2	86.2(3)	O(9)#5-In(3)-O(20)#6	103.9(3)
O(20)#6-In(3)-O(8)#7	134.4(2)	O(9)#5-In(3)-O(8)#7	88.6(3)
O(9)#5-In(3)-O(16)	84.6(3)	O(16)-In(3)-O(7)#7	96.2(2)
O(20)#6-In(3)-O(16)	142.6(2)	O(15)-In(3)-O(7)#7	87.1(2)
O(8)#7-In(3)-O(16)	81.3(2)	O(9)#5-In(3)-O(19)#6	83.5(3)
O(9)#5-In(3)-O(15)	121.1(2)	O(20)#6-In(3)-O(19)#6	57.2(2)
O(20)#6-In(3)-O(15)	87.9(2)	O(8)#7-In(3)-O(19)#6	81.7(2)
O(8)#7-In(3)-O(15)	123.0(2)	O(16)-In(3)-O(19)#6	159.5(2)
O(16)-In(3)-O(15)	57.8(2)	O(15)-In(3)-O(19)#6	142.5(2)
O(9)#5-In(3)-O(7)#7	145.3(3)	O(7)#7-In(3)-O(19)#6	84.4(2)
O(20)#6-In(3)-O(7)#7	96.4(2)	O(8)#7-In(3)-O(7)#7	57.5(2)

Symmetry transformations used to generate equivalent atoms:

#1 -x-1/2,-y-1/2,z #2 x+1/4,-y-3/4,z+1/4 #3 x-1/4,-y-3/4,z-1/4 #4 -x-3/4,y-1/4,z+3/4

#5 -x-3/4,y+1/4,z-3/4 #6 -x-3/4,y+1/4,z+1/4 #7 -x-1/2,-y-1/2,z-1 #8 -x-1/2,-y-1/2,z+1

Table S7. Selected bond lengths [Å] and angles [º] for compound **JLU-Liu6**.

Zn(1)-O(12)	1.976(3)	Zn(2)-O(4)	1.850(4)
Zn(1)-O(7)#1	2.020(3)	Zn(2)-O(11)	1.902(5)
Zn(1)-O(8)#2	2.023(3)	Zn(2)-O(1)#5	2.012(12)
Zn(1)-O(6)#3	2.034(3)	Zn(2)-O(4)#4	2.027(4)
Zn(1)-O(5)	2.040(3)	Zn(2)-O(1')#5	2.322(17)
Zn(3)-O(3)	2.057(6)	Zn(4)-O(11)	1.759(4)
Zn(3)-O(13)	2.091(12)	Zn(4)-O(10')#7	1.930(5)
Zn(3)-O(2')#5	2.129(9)	Zn(4)-O(9)#6	1.930(7)
Zn(3)-O(1')#5	2.332(18)	Zn(4)-O(2)#5	1.935(6)
Zn(3)-O(1)#5	2.362(14)	Zn(4)-O(10)#7	1.960(18)
Zn(3)-O(11)	2.3879(14)	Zn(3)-O(9')#6	2.011(7)
O(12)-Zn(1)-O(7)#1	99.68(16)	O(13)-Zn(3)-O(1)#5	111.1(5)
O(12)-Zn(1)-O(8)#2	102.06(15)	O(2')#5-Zn(3)-O(1)#5	54.8(4)
O(7)#1-Zn(1)-O(8)#2	158.23(15)	O(1')#5-Zn(3)-O(1)#5	15.9(4)
O(12)-Zn(1)-O(6)#3	100.90(16)	O(9')#6-Zn(3)-O(11)	91.4(3)
O(7)#1-Zn(1)-O(6)#3	88.72(15)	O(3)-Zn(3)-O(11)	84.2(2)
O(8)#2-Zn(1)-O(6)#3	88.33(16)	O(13)-Zn(3)-O(11)	169.6(5)
O(12)-Zn(1)-O(5)	100.92(16)	O(2')#5-Zn(3)-O(11)	95.0(3)
O(7)#1-Zn(1)-O(5)	86.61(16)	O(1')#5-Zn(3)-O(11)	88.2(5)
O(8)#2-Zn(1)-O(5)	88.14(17)	O(1)#5-Zn(3)-O(11)	74.0(3)
O(6)#3-Zn(1)-O(5)	158.15(15)	O(9')#6-Zn(3)-O(3)	108.9(3)
O(4)-Zn(2)-O(11)	125.52(17)	O(9')#6-Zn(3)-O(13)	88.6(5)
O(4)-Zn(2)-O(1)#5	108.0(3)	O(3)-Zn(3)-O(13)	85.9(5)
O(11)-Zn(2)-O(1)#5	93.8(3)	O(9')#6-Zn(3)-O(2')#5	97.1(4)
O(4)-Zn(2)-O(4)#4	111.3(2)	O(3)-Zn(3)-O(2')#5	154.0(3)
O(11)-Zn(2)-O(4)#4	116.17(14)	O(13)-Zn(3)-O(2')#5	95.3(6)
O(1)#5-Zn(2)-O(4)#4	94.1(4)	O(9')#6-Zn(3)-O(1')#5	155.9(5)
O(4)-Zn(2)-O(1')#5	93.0(3)	O(3)-Zn(3)-O(1')#5	95.0(4)
O(11)-Zn(2)-O(1')#5	101.5(4)	O(13)-Zn(3)-O(1')#5	96.0(6)
O(1)#5-Zn(2)-O(1')#5	15.2(4)	O(2')#5-Zn(3)-O(1')#5	59.0(4)
O(4)#4-Zn(2)-O(1')#5	102.0(5)	O(9')#6-Zn(3)-O(1)#5	145.7(4)
O(11)-Zn(4)-O(10')#7	115.45(18)	O(3)-Zn(3)-O(1)#5	100.5(3)
O(11)-Zn(4)-O(9)#6	110.2(3)	O(11)-Zn(4)-O(10)#7	116.4(5)
O(10')#7-Zn(4)-O(9)#6	101.6(4)	O(10')#7-Zn(4)-O(10)#7	28.9(5)
O(11)-Zn(4)-O(2)#5	105.9(2)	O(9)#6-Zn(4)-O(10)#7	74.3(6)
O(10')#7-Zn(4)-O(2)#5	115.3(3)	O(2)#5-Zn(4)-O(10)#7	133.9(6)
O(9)#6-Zn(4)-O(2)#5	108.2(3)		

Symmetry transformations used to generate equivalent atoms:

#1 -x+3/2,y+1/2,-z+3/2 #2 x,-y+1,z-1/2 #3 -x+3/2,-y+3/2,-z+1 #4 -x+1,y,-z+3/2 #5 x,-y+1,z+1/2 #6 x,y+1,z #7 -x+1,y+1,-z+3/2 #8 -x+3/2,y-1/2,-z+3/2 #9 x,y-1,z #10 -x+1,y-1,-z+3/2

Reference:

1. G. M. Sheldrick, SHELXTL-97, Program for Crystal Structure Refinement, University of Gottingen, 1997.
2. A. L. Spek, *J. Appl. Crystallogr.* 2003, **36**, 7-13.
3. *(a)* M. O'Keeffe, O. M. Yaghi, *Chem. Rev.* 2012, **112**, 675-702; *(b)* Z. Guo, H. Wu, G. Srinivas, Y. Zhou, S. Xiang, Z. Chen, Y Yang, W. Zhou, M. O'Keeffe, B. Chen, *Angew. Chem., Int. Ed.* 2011, **50**, 3178-3187; *(c)* Y. Liu, J. F. Eubank, A. J. Cairns, J. Eckert, V. Ch. Kravtsov, R. Luebke, M. Eddaoudi, *Angew. Chem., Int. Ed.* 2007, **46**, 3278-3283. *(d)* D. Zhao, D. Yuan, A. Yakovenko, H.-C. Zhou, *Chem. Commun.*, 2010, **46**, 4196-4198.
4. J. L. C. Rowsell, O. M. Yaghi, *J. Am. Chem. Soc.* 2006, **128**, 1304-1315.
5. D. M. Ruthven, *Principles of Adsorption and Adsorption Processes*; *Wiley: New York,* 1984.
6. A. L. Myers, J. M. Prausnitz, *AIChE J.* 1965, **11**, 121-127.
7. Z. H. Xiang, X. Peng, X. Cheng, X. J. Li and D. P. Cao, J. Phys. Chem. C, 2011, **115**, 19864-19871.
8. Y. S. Bae, O. K. Farha, J. T. Hupp and R. Q. Snurr, *J. Mater. Chem*., 2009, **19**, 2131-2134.
9. Z. Zhang, S. Xiang, K. Hong, M. C. Das, H. D. Arman, M. Garcia, J. U. Mondal, K. M. Thomas, B. Chen, *Inorg. Chem.* 2012, **51**, 4947-4953.
10. T. Ben, Y. Q. Li, L. K. Zhu, D. L. Zhang, D. P. Cao, Z. H. Xiang, X. D. Yao and S. L. Qiu, *Energy Environ. Sci*., 2012, **5**, 8370-8376.
11. Z. Zhang, S. Xiang, Y.-S. Chen, S. Ma, Y. Lee, T. Phely-Bobin, B. Chen, *Inorg. Chem.* 2010, **49**, 8444-8448.
12. S. D. Burd, S. Ma, J. A. Perman, B. J. Sikora, R. Q. Snurr, P. K. Thallapally, J. Tian, L. Wojtas, M. J. Zaworotko, *J. Am. Chem. Soc*., 2012, **134**, 3663-3666.
13. B. Mu, F. Li, K.S. Walton, *Chem. Commun.* 2009, **18**, 2493-2495.
14. P. S. Nugent, V. L. Rhodus, T. Pham, K. Forrest, L. Wojtas, B. Space, M. J. Zaworotko, *J. Am. Chem. Soc*., 2013, **135**, 10950-10953.
15. M. Heuchel, G. M. Davies, E. Buss and N. A. Seaton, *Langmuir*, 1999, **15**, 8695-8705.
16. R. Babarao, Z. Q. Hu, J. W. Jiang, S. Chempath and S. I. Sandler, *Langmuir*, 2007, **23**, 659-666.
17. X. H. Shao, Z. H. Feng, R. S. Xue, C. C. Ma, W. C. Wang, X. Peng and D. P. Cao, *AIChE J*., 2011, **57**, 3042-3051.